Optical-Feedback Cavity Ring-Down Spectroscopy Measurements of Extinction by Aerosol Particles†

Timothy J.A. Butler, Daniel Mellon, Jin Kim, Jessica Litman,‡ and Andrew J. Orr-Ewing*

School of Chemistry, University of Bristol, Cantock's Close, Bristol BS8 1TS, United Kingdom

Received: November 24, 2008; Revised Manuscript Received: January 16, 2009

Optical feedback cavity ring-down spectroscopy (OF-CRDS) using a continuous wave distributed feedback diode laser at 1650 nm has been used to measure extinction of light by samples of monodisperse spherical aerosol particles $<1\ \mu$m in diameter. The OF-CRDS method allows measurements of low levels of extinction of incident light to be made at repetition rates of 1 kHz or greater. A statistical model is proposed to describe the linear relationship between the extinction coefficient (α) and its variance ($Var(\alpha)$). Application of this model to experimental measurements of $Var(\alpha)$ for a range of α values typically below $\sim 1 \times 10^{-6}$ cm^{-1} allows extinction cross-sections for the aerosol particles to be obtained without need for knowledge of the particle number density. Samples of polystyrene spheres with diameters of 400, 500, 600, and 700 nm were used to test the model by comparing extinction cross-sections determined from the experiment with the predictions of Mie theory calculations. Fitting of ring-down decay traces exhibiting amplitude noise to extract cavity ring-down times introduces additional quadratic and higher order polynomial dependencies of the variance that become significant for larger particle number densities and thus extinction coefficients (typically for $\alpha > 1 \times 10^{-6}$ cm^{-1} under our experimental conditions). Aggregation of particles at larger number densities is suggested as a further source of variance in the measurements. Extinction cross-sections are severely underestimated if the measurements are made too rapidly to sample uncorrelated distributions of particle numbers and positions.

1. Introduction

Atmospheric aerosols arise from both natural sources, such as volcanic dust and mineral salts, and anthropogenic activity, including burning of biomass and fossil fuels.[1] Aerosol particles in the atmosphere affect the Earth's radiation budget both directly, by scattering or absorption of sunlight, and indirectly, by acting as cloud condensation nuclei. Unlike long-lived greenhouse gases such as CO_2 and CH_4, which have radiative forcing (RF) values determined to high precision (+2.63 [±0.26] W m^{-2}),[1] the effects of aerosols on radiation budgets are still poorly quantified. According to the Fourth Assessment of the Intergovernmental Panel on Climate Change (IPCC),[1] total direct aerosol RF amounts to −0.5 [±0.4] W m^{-2}, with a medium-to-low level of scientific understanding, and the RF caused by cloud albedo is −0.7 [−1.1, +0.4] W m^{-2}, with a low level of scientific understanding. The effect of cloud albedo is the key uncertainty in evaluating the RF of the Earth's climate. The optical properties of atmospheric aerosols must therefore be subjected to further detailed scrutiny to enable accurate predictions of their effects on the Earth's radiation budget.

Since its initial demonstration,[2] cavity ring-down spectroscopy (CRDS) has developed into a widely used technique to measure absolute optical extinctions, particularly at very low levels where traditional spectroscopic techniques fail. The methods and applications of CRDS have been extensively reviewed by various authors.[3−10] Light from a laser source is injected into a high-finesse optical cavity constructed from two or more mirrors of very high reflectivities. In a stable cavity, the light is reflected back and forth many thousands of times between the mirrors, giving a long effective path length over which weak extinction losses can be measured. The extinction losses caused by scattering and absorption from a sample confined within the cavity can be deduced from the rate of exponential decay of light intensity leaking from the cavity through the mirrors. The ring-down time (τ) is defined as the time interval in which the intensity of light decreases by a factor of 1/e and is the reciprocal of the rate coefficient (k) for the exponential decay. To date, CRDS has found greatest application in the study of gaseous samples[3−10] but has recently been increasingly applied to the study of aerosols,[11−30] sometimes in conjunction with other techniques such as nephelometry.[18,22] Various aerosol types have been studied, ranging from nonabsorbing (e.g., water,[23] inorganic salts,[14,24,25] polystyrene beads[16,26,27]) to absorbing samples (e.g., soot,[21] organic aerosols[24,25]). Mixed composition aerosols have also been investigated to test mixing rules for extinction properties.[28]

CRDS of aerosols measures the total extinction by the sample of particles contained within the optical cavity; this extinction is the sum of scattering and absorption losses. Various strategies have been developed to separate the contributions from the real and complex parts of the refractive indices of the particles, including measurement of extinction efficiencies (Q_{ext}) for various size parameters $x = 2\pi r/\lambda$ and comparison with Mie scattering calculations.[25,28−30] The measured extinction depends on the number of particles within the volume of the intracavity laser beam, and the statistics of spatial distributions of aerosol particles have been discussed by Larsen.[31] Fluctuations in the number of particles within the beam result in rapid changes in the measured extinction and become more pronounced at low

† Part of the "George C. Schatz Festschrift".

* To whom correspondence should be addressed. Phone: +44 117 928 7672. Fax: +44 117 925 0612. E-mail: a.orr-ewing@bris.ac.uk.

‡ Permanent address: Department of Chemistry, Queen's University, Kingston, Ontario, K7L 3N6, Canada.

10.1021/jp810310b CCC: $40.75
Published on Web 02/27/2009

particle number densities. Such fluctuations are negligible for most studies of gaseous samples (e.g., for detection of 10 pptv of a trace atmospheric constituent in ambient air, $\sim 10^7$ molecules will be within the intracavity laser volume) but can have significant impact on the precision of aerosol extinction measurements by CRDS because there might only be 100−1000 particles on average within the probe volume. Pettersson et al.[16] quantified this effect by examining the Poisson statistics of the number of aerosol particles sampled by their CRDS measurements and derived a relationship between the extinction coefficient, α, and its standard deviation, σ_α

$$\sigma_\alpha = \sqrt{\frac{\alpha^2}{nVRt} + \alpha_{\min}^2} \quad (1)$$

Here n is the aerosol number density, V is the effective laser beam volume in the ring-down cavity, R is the repetition rate at which measurements are made, and t is the time over which data are accumulated. $\alpha_{\min}$ is the limiting extinction coefficient determined by noise inherent in the experimental apparatus in the absence of the aerosol sample. The standard deviations of extinction coefficient measurements were determined for a range of particle sizes and number densities, and the data were well described by eq 1, but quantitative agreement required use of a value for V that was a factor of 5 smaller than that expected for a Gaussian TEM_{00} mode within the cavity.

Bulatov et al.[24] adopted a similar statistical approach to analyze the variations in extinction for a variety of size-selected aerosol particles. They noted that relative fluctuations in the extinction coefficient vary reciprocally with the square root of the number of particles (N) in the system

$$\frac{\alpha}{\sigma_\alpha} = \sqrt{NV} \quad (2)$$

Values of N were separately determined by a condensation particle counter, and plots of α/σ_α against $\sqrt{N}$ were observed to be linear but with gradients that depended on the sample type (composition and refractive index). Similar discrepancies were noted, however, to those of Pettersson et al.[16] in the determined values of V. Possible reasons for these discrepancies will be discussed later in this paper.

Many implementations of CRDS, including most of the above examples, used pulsed laser sources and thus have the associated disadvantage that the data acquisition rate is limited by the repetition rate of the laser. CRDS with continuous wave (CW) diode lasers enables higher measurement rates, typically up to ~200 Hz.[32] Strawa et al. were the first to apply CW laser CRDS to the study of aerosols.[15] The recent development of optical feedback cavity ring-down spectroscopy (OF-CRDS) by Morville et al.[33] now enables kHz measurement rates and has the further advantage that it requires a low-cost distributed feedback (DFB) diode laser. In OF experiments, a fraction of light leaking from the optical cavity is returned to the laser. This feedback light locks the frequency of the laser to a cavity mode and narrows the laser bandwidth, thus enhancing the efficiency of coupling of laser light into the high-finesse cavity. Romanini and co-workers used OF-CRDS and related methods to measure absorption by a variety of trace atmospheric gases.[33,34,34−36] We previously demonstrated the use of OF-CRDS to measure extinction by individual, micrometer-sized aerosol particles and demonstrated that the scattering of light depends on the radial and axial positions of the particle within the laser beam.[26,27]

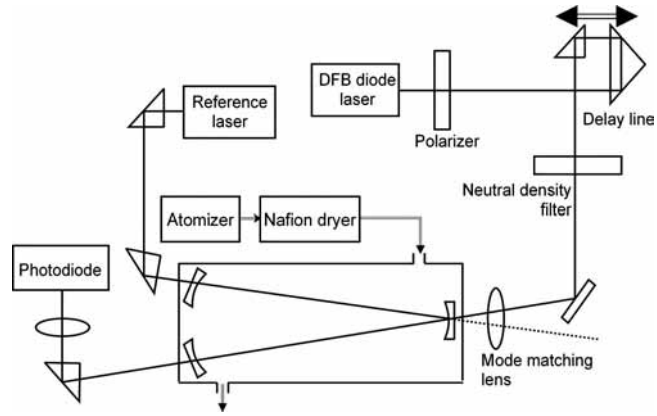

Figure 1. Schematic diagram of the experimental setup for the OF-CRDS study of the optical properties of aerosols: DFB = distributed feedback diode laser.

The method is potentially well suited for the study of ensembles of aerosol particles of low number density if the fast data acquisition rate allows rapid accumulation of statistical information on fluctuations in extinction caused by variation of the small number of particles in the probe laser volume.

In this paper, we demonstrate the use of OF-CRDS to measure extinction by samples of monodisperse, spherical aerosol particles with diameters less than 1 μm. The OF-CRDS setup and experimental technique are briefly described, and a modified statistical model is presented, which can be used to extract the extinction cross-sections of individual particles without prior knowledge of the particle number density, a key difference from prior studies. Conditions under which the measurements are reliable are examined using computational simulations. The quantitative retrieval of aerosol particle optical properties is then tested by comparing experimentally determined extinction cross-sections with calculations using Mie theory. The consequences of variance in the measured extinction arising from other sources, including a distribution of particle sizes, and the fits to ring-down decay data are also examined.

2. Experimental Section

Figure 1 shows a schematic diagram of the experimental setup used for OF-CRDS measurements. The apparatus is similar to that described previously for study of single aerosol particles,[26] and only a brief description is given here. A CW DFB diode laser operating at 1650 nm was used as the light source, and the optical cavity consisted of three plano-concave mirrors (1 m radius of curvature, reflectivity $R = 0.99988$ at 1650 nm) arranged in a V shape. The two cavity arms were initially 30 cm long, giving a free spectral range (FSR) of 250 MHz. In later experiments, reconstruction of the cavity resulted in arm lengths of 31.5 cm. The angle between the two cavity arms was 11°. The cavity was housed within a box that was sealed apart from entry and exit ports for flow of aerosol particles; the exit port flow passed through a filter to the surrounding atmosphere. Light from the laser was injected into the ring-down cavity via the central (input) mirror, and the laser switched on and off at a rate of 1.25 kHz using a square-wave voltage pulse to the laser driver. When the laser turned on, its frequency underwent a chirp that swept through several free spectral ranges (FSRs) of the ring-down cavity. As the chirp rate slowed toward the end of each pulse, light build-up in the cavity caused feedback and locking of the laser to a cavity mode frequency. Ring-down events were recorded at the end of each pulse, when the laser operating current was switched below threshold.

Excitation of TEM_{00} modes of the cavity, but not higher order transverse modes, was ensured by careful alignment of the injected laser beam and cavity mirrors, together with monitoring of the pattern of intensity transmitted by the cavity as the laser frequency was scanned.

The advantage of using a V-shaped cavity[33,34] is that the initial reflection of the incoming laser beam from the input mirror is deflected away from the return path to the laser, so only light circulating in the cavity and thus in resonance with a cavity mode returns to the laser and causes optical feedback. The feedback rate was controlled by manual positioning of a continuously variable neutral density filter (Thorlabs, optical density 0.04−2.0). As cavity losses increased (because of extinction by intracavity samples), the position of the neutral density filter was adjusted, as necessary, from its setting for an empty cavity to reduce attenuation and thus maintain stable feedback between the cavity and diode laser.

Optimal optical feedback requires fine control of the phases of the light incident on the cavity and the light returning to the laser. Successive cavity modes (odd and even) alternatively present a node and an antinode at the input mirror and result in slightly different reflectivity and losses. Therefore, in order to have the same optical feedback phase for all modes, the laser−cavity distance was set to an odd multiple of the cavity arm length.[34] In our case, the laser−cavity distance was first manually adjusted to approximately 90 cm (later 94.5 cm) then finely adjusted using a delay line, which consisted of a prism mounted on a piezoelectric transducer (PZT). The PZT mount was controlled by a feedback circuit, which sent an error signal when the OF phase was above or below the optimal point. A photodiode detected the light escaping through the output mirror. The photodiode signals were digitized by a data acquisition card (Gage CS1450, 14-bit, 50 MS/s) and then analyzed by a custom written LABVIEW program using a fast Fourier transform (FFT) fitting procedure for the exponential ring-down decays.[37]

A dilute suspension of polystyrene spheres (PSS, Duke Scientific Corp.) in distilled water was nebulized, with a backing pressure of ∼0.3 bar above atmospheric pressure. Since PSS particles are nonabsorbing at 1650 nm, they provide a good scattering model. The generated aerosols were flowed through a Nafion dryer (PD-100T-12MSS, Perma Pure) to remove moisture before entering the chamber. At the exit, a HEPA filter was used to remove all aerosol particles. Several background ring-down times were taken with an empty cavity, and then the chamber was subjected to a continuous flow of aerosol particles for about 30 min until equilibrium was reached, at which point the flow was terminated. Measurements of ring-down times and corresponding standard deviations were then taken periodically as the particles settled by gravitation. Ring-down times increased with decreasing particle concentration, and measurements were taken until the ring-down returned to close to the background value. In some cases, an alternative approach was used in which measurements were made as the aerosol particles were introduced to the chamber. The aerosol particles occupied all parts of the chamber, and thus the entire region between the cavity mirrors, but they did not need to be uniformly distributed for the purposes of the measurements. As our results will demonstrate, no mechanical stirring of the particles was required.

Typical background ring-down times were ∼8.0 μs with a standard deviation of 0.03 μs for averaging of 500 events at an accumulation rate of 1.25 kHz, which gave a value of $\alpha_{min} = 1.5 \times 10^{-8}$ cm^{-1} (or 9.5×10^{-9} cm^{-1} Hz$^{-1/2}$) for the minimum detectable extinction coefficient. This value is taken to represent the baseline noise level and is too large for observation of the scattering by single particles of diameters <1 μm (although use of a visible rather than near-IR laser would permit extension of such studies to smaller particle sizes). For each of the sets of 500 measurements, acquired in 0.4 s, the average extinction coefficient, $\langle\alpha\rangle$, and its variance, $Var(\alpha)$, were determined. The development of the methods of data analysis considers total extinction and is thus not specific only to either scattering or absorption losses.

3. Theory

Before presenting the results of the measurements of $\langle\alpha\rangle$ and $Var(\alpha)$, we develop a model linking the two properties that is based on the Poisson statistics of fluctuating numbers of particles within the volume of the TEM_{00} mode of the optical cavity. This model was tested using computer simulations that demonstrate clearly the circumstances under which the method can be successfully applied.

3.A. Statistical Model for the Fluctuations in the Measured Extinction. ***3.A.1. Statistical Variation of the Number of Particles in the Intracavity Laser Beam.*** In the following analysis, we treat the intracavity laser beam as being cylindrical along each arm of the V-shaped cavity. The partial focusing of the beam within the cavity is discussed in section 3.A.3. We previously showed that the variances of the extinction for a uniform intensity cylindrical beam of radius r_0 and a cylindrical beam with Gaussian power profile described by a beam radius w, defined such that the radial (r-dependent) profile is $I(r) = I(r = 0) \exp(-2r^2/w^2)$, are the same provided the choice $r_0 = w$ is made for the former case.[26] The analysis thus focuses initially on the simpler case of a uniform cylindrical beam. Modifications to incorporate a Gaussian beam profile are then discussed. In what follows, we use L_{cav} and L to denote, respectively, the total length of the optical cavity and the length of one arm of the symmetric V-shaped cavity (such that $L_{cav} = 2L$).

In the V-shaped cavity employed in our experiments, the central mirror has a curved reflective surface and we therefore evaluate properties of the TEM_{00} cavity mode such as its radius and volume by treating it as two separate cavities of length L instead of a single cavity of length $2L$. This approach is borne out by the measurements of the beam waist in the center of one cavity arm reported previously;[26] the value obtained is better matched by consideration of two 30 cm long cavities than by calculations for a single cavity of length 60 cm in which the additional focusing by the central mirror is not taken into account.

We define the volume occupied by a cavity mode as $V = 2\pi r_0^2 L$, where, as indicated above, the chosen value of r_0 will be determined by w for a TEM_{00} cavity mode. Each particle within the cavity mode volume experiences an intensity i that, for a uniform beam, is independent of its position

$$i(r, z) = \frac{I_z}{\pi r^2} \tag{3}$$

In eq 3, I_z is the total power of the beam at a distance z along the central axis of the cavity. For a uniform cylindrical beam, there is no z dependence to the power and we write $I_z = I$. The subtle effects on measured extinction caused by the longitudinal standing-wave structure of the light inside a cavity excited by a CW laser were considered in detail by Miller and Orr-Ewing[27] and are discussed in section 3.A.4.

The average extinction coefficient of an ensemble of particles in the volume of the laser beam is equal to the average of the

sum of the extinction coefficients of the N individual particles

$$\langle\alpha\rangle = \left\langle \sum_{j=1}^{N} \left(\frac{\sigma_j i_j}{Il}\right)\right\rangle = \frac{2L}{l} n\sigma \tag{4}$$

where σ_j is the extinction cross-section of the jth particle (and for equivalent particles $\sigma_j = \sigma$), i_j is the light intensity experienced by that particle, and l is the distance within the cavity over which the aerosol sample extends. The number density of aerosol particles is denoted by n ($n = N/V$). The extinction coefficient is defined by $\alpha = \varepsilon/l$, where ε denotes the extinction per pass through the cavity.

The fluctuations in the number of particles in the beam at any one time can be described using Poisson statistics, with the mean and variance given by N. From eq 4, the variance in the extinction coefficient can be derived as

$$Var(\alpha) = \left(\frac{2L\sigma}{Vl}\right)^2 N = \frac{2\sigma^2 nL}{\pi r_0^2 l^2} \tag{5}$$

If the distribution of particles is (macroscopically) uniform over the entire beam cavity length, $l = L_{cav} = 2L$ and

$$Var(\alpha) = \frac{\sigma}{V}\langle\alpha\rangle \tag{6}$$

which also applies for a cylindrical beam with Gaussian power profile if we take $V = 2\pi w^2 L$.[26] The total variance in the experimental measurements of α is the sum of the variances that are introduced by various contributing factors that include the statistical fluctuation in the number density of particles within the laser beam volume and the inherent noise associated with the experimental setup. The latter contribution could arise from mechanical instabilities, detector noise, or shot noise. Variance in α also derives from the size distribution of particles but, as is shown below, is small enough to be considered negligible for the manufactured PSS particles used in this investigation. In a preliminary analysis of the size-distribution effects, we erroneously attributed a contribution to $Var(\alpha)$ that was quadratic in $\langle\alpha\rangle$.[38] Taking into account the above factors, but with neglect of particle size distribution effects, we can write

$$Var(\alpha) = \frac{\sigma}{V}\langle\alpha\rangle + \alpha_{min}^2 \tag{7}$$

where α_{min} is the minimum detectable extinction coefficient, determined by the inherent noise in the system as described above. A plot of $Var(\alpha)$ against $\langle\alpha\rangle$ should therefore give a straight line with gradient equal to σ/V. Such an analysis requires data from measurements of $\langle\alpha\rangle$ recorded at different particle densities and under conditions where Poisson statistics apply, but the number densities do not need to be known in order to determine σ.

3.A.2. Effects of a Distribution of Particle Sizes. If the sample of spherical particles is not monodisperse, the distribution of the sizes will contribute to the measured variance of the extinction coefficient. The extinction cross-section is related to the geometric cross-section ($\sigma_{geom} = \pi(d/2)^2$) of the particles of diameter d by $\sigma = Q_{ext}\sigma_{geom}$, where Q_{ext} is the size-dependent extinction efficiency. Over a small size range centered on a mean diameter d_0, we can approximate Q_{ext} as being a linear function of d

$$Q_{ext}(d) = Q_{ext}(d_0) + (d - d_0)q \tag{8}$$

where q is a constant and $Q_0 = Q_{ext}(d_0)$ is the extinction efficiency for the mean diameter particles. We obtain the contribution to the variance in the extinction coefficient from a distribution of particle diameters with variance $Var(d)$ to be

$$Var_d(\alpha) = \langle\alpha\rangle\left(\frac{\pi}{4VQ_0}\right)(qd_0 + 2Q_0)^2 Var(d) \tag{9}$$

with the subscript d emphasizing that this is just one contribution to the total variance. This term can be evaluated for specified distributions of particle sizes and incorporated into models for analysis of the experimentally measured variance of the extinction coefficient. For representative nearly monodisperse polystyrene spheres employed in our experiments with $d_0 = 707$ nm and $Var(d) = 75$ nm^2 and estimates of the values of q and Q_0 from Mie scattering calculations, the contribution to the total variance in α from the size distribution is found to be negligible: evaluation of eq 9 for these particles with a mean extinction $\langle\alpha\rangle = 1 \times 10^{-6}$ cm^{-1} and $Q_0 = 0.76$ and $q = 0.0031$ nm^{-1} at $\lambda = 1650$ nm results in $Var_d(\alpha) = 2.8 \times 10^{-17}$ cm^{-2}. Over the range of particle sizes used in our experiments, the approximation of linear variation of Q_{ext} with d is confirmed by Mie scattering calculations. The value of $Var_d(\alpha)$ is a factor of $\sim$200 smaller than the variance caused by fluctuations of the number of particles within the volume of the TEM_{00} mode and can thus be discounted. A size range of $\pm$150 nm about d_0 is necessary for the value of $Var_d(\alpha)$ to match that from the particle number fluctuations. Size selection using a differential mobility analyzer (DMA) prior to the types of experiment described here is thus a practical option for measurements of extinction of naturally occurring aerosol particles with a broad distribution of diameters.

3.A.3. Volume of the TEM_{00} Cavity Mode. Within a linear optical cavity, excitation of a TEM_{00} mode results in a cylindrically symmetric Gaussian distribution of intracavity light, $i(r,z)$, at any axial position z that is given by

$$i(r,z) = \frac{2I}{\pi w_z^2}\exp\left(-2\frac{r^2}{w_z^2}\right) \tag{10}$$

Here I is the total power of the intracavity beam and w_z is the beam radius at a particular z value. The beam radius is defined as the distance from the center at which the intracavity field has decayed to 1/e of its maximum value and is a minimum (w_0) at the beam waist, which, for a symmetrical optical resonator, lies at the center of the cavity. The beam, of wavelength λ, diverges from the beam waist with dependence[39]

$$w_z = w_0\sqrt{1 + \left(\frac{z\lambda}{\pi w_0^2}\right)^2} \tag{11}$$

If, as discussed earlier, we treat our V-shaped cavity as a pair of linear cavities, each of length L, and neglect the effects of the very small overlap of the beams in the two cavity arms in the vicinity of the central mirror, the volume of the mode lying within a radius w_z is

$$V_{tot} = 2\pi w_0^2 L\left(1 + \frac{1}{12}\left(\frac{L\lambda}{\pi w_0^2}\right)^2\right) \quad (12)$$

This expression differs by the second term from the value we have so far used for the cavity mode volume, $V = 2\pi w_0^2 L$, which neglects the z dependence of w_z. For the parameters described in section 2, $w_0 = 0.433$ mm and eq 12 gives $V_{tot} = 0.374$ cm^3. The volume obtained without inclusion of the second term in eq 12 is $V = 0.354$ cm^3, which is 5% smaller. The correct value of V_{tot} can, in principle, be used to compute the theoretical expectation of the gradient of plots of the form of eq 7 in place of the approximate use of $V = 2\pi w_0^2 L$. We note, however, that eq 7 was derived with the approximation of a purely cylindrical beam (i.e., the beam waist is constant along the cavity length). In the case of the optical cavity used in our experiments, the Gaussian beam radius at the two cavity end mirrors is calculated to be 0.470 mm and thus differs by only 8% from the beam waist in the center of each arm, suggesting that the approximation of a purely cylindrical beam is robust.

Scattering of the light from the TEM_{00} mode might, in principle, couple intracavity intensity into higher order transverse modes of the cavity and thus not constitute a cavity loss. These higher order modes are, in general, not resonant with the TEM_{00} mode however, and Doppler shifts induced in the scattered light frequencies by motions of the particles are estimated to be less than 1 MHz (i.e., smaller than the laser band width and much less than the cavity free spectral range of ~250 MHz). Although the light is mostly scattered in the forward direction, for the small particles studied here, the probability of light being sufficiently forward scattered to be retained within the ring-down cavity is estimated to be negligibly small. We thus discount the possibility of systematic errors resulting from excitation of higher order modes by intracavity light scattering.

3.A.4. Longitudinal Cavity Mode Structure. Excitation of a TEM_{00} cavity mode establishes a standing wave between the two cavity end mirrors with nodes and antinodes along each arm of the V-shaped cavity. Miller and Orr-Ewing[27] demonstrated that the extinctions caused by particles depend on their positions relative to the standing wave structure of the cavity mode, with the effects being most pronounced for particles with diameters (d_p) comparable to the wavelength (λ) of the light within the cavity (and thus size parameters $x_p \approx 1$ ($x_p = \pi d_p/\lambda$). A phase parameter $\zeta(z_0)$ was introduced to quantify the ratio of extinction efficiencies, Q_{ext}, for a particle in a standing wave in an optical cavity and for regular Mie scattering of an incident traveling plane wave by the same particle. Here, z_0 is the phase of the standing wave with respect to the center of the particle, with $z_0 = 0$ and $\lambda/4$, respectively, denoting a particle centered on an extremum or a node. The dependence of measured extinction coefficients on z_0 will add variance to data sets that is not amenable to straightforward analytical quantification but may be significant in a regime such as occurs in our experiments in which particles with $x_p \approx 1$ are being studied. Although for a distribution of particles with random phases z_0, the phase parameter ζ should average to $\langle\zeta\rangle \approx 1$, there will be differences in the value of $\langle\zeta\rangle$ for each experimental determination of cavity loss that contribute to $Var(\alpha)$. We have not attempted to quantify these contributions further because the outcomes of experimental measurements presented in section 4 suggest that for ~10^2−10^3 particles lying within the cavity mode for any one measurement of cavity losses, the resultant contribution to $Var(\alpha)$ is small. The validity of neglecting the effects of the phase parameter could, however, be tested further by computer simulation, as could the possible distortion of ring-down decays from a single-exponential form resulting from motion of particles along the cavity mode axis on the time scale of the ring-down measurement.[27]

3.A.5. Conditions under which the Poisson Statistical Analysis Applies. The experimental studies presented in this paper test the use of eq 7 to derive accurate values for the extinction cross-sections for spherical aerosol particles. The correct measurement of the variance of the extinction is a key part of this process; if sequential measurements of $Var(\alpha)$ are correlated, the model will break down. Likewise, if the fluctuations in the number of particles do not follow Poisson statistics, the analysis in section 3.A.1 will be invalid.

If we consider a projection of the particles distributed over a range of z values into a plane perpendicular to the optical cavity axis, we can compare the total cross-section of all the particles to the cross-sectional area of the cavity mode. The ratio of total-particle to cavity-mode cross-sectional areas is much less than unity under the conditions of low light extinction employed in our experiments. If we imagine each aerosol particle occupies a circular box of diameter $2d$ (to exclude overlap of two particles) and consider 700 nm diameter particles, the number of such boxes that fit into the cross-sectional area of the laser beam at its narrowest point is ~5×10^5. If we have ~500 particles in the beam at one time, only 0.1% of the boxes are occupied, satisfying the Poisson condition for rare events, and the probabilities of multiple scattering will be negligibly small. The application of a Poisson statistical analysis also requires that the locations of the particles change sufficiently quickly that sequential measurements of light extinction probe independent distributions of particles (i.e., the correlation time is less than the measurement interval). This point is discussed further below and will be satisfied if the transit times of the particles through the cavity mode are less than the time between measurements.

The principle of projection of all the particles into a plane to calculate total extinction also served as the basis for our computer simulations of the measured variances. This projection is appropriate if the particles scatter light from the cavity in a way that is taken to be independent of their z coordinate. Such an assumption is a simplification (see section 3.A.4)[27] but should not have significant consequences for the analysis that follows. A simulation was developed to compute the extinction per pass, ε, for each of an ensemble of particles, with due allowance for the radial position relative to the central axis of a Gaussian TEM_{00} mode with beam radius w. As demonstrated by Butler et al.,[26] the single-particle extinction is

$$\varepsilon = \frac{2\sigma}{\pi w^2} e^{\frac{-2r^2}{w^2}} \quad (13)$$

and can be converted to an extinction coefficient using $\alpha = \varepsilon/L_{cav}$ (if, as in our experiments, the particles occupy the entire region between the cavity mirrors, so $l = L_{cav}$). The simulations randomly select the coordinates of all particles and then allow their positions to evolve in 3 dimensions with time through Brownian motion and gravitational settling. At each time step, the extinction coefficient of each particle is evaluated using eq 13 and the total extinction coefficient is obtained by summation. The velocity components along z are included to treat the 3-D particle motion correctly, but the recalculation of extinctions neglects any changes to the z coordinate.

During each time step, the particles move in a direction determined by the resultant of the Brownian and gravitational

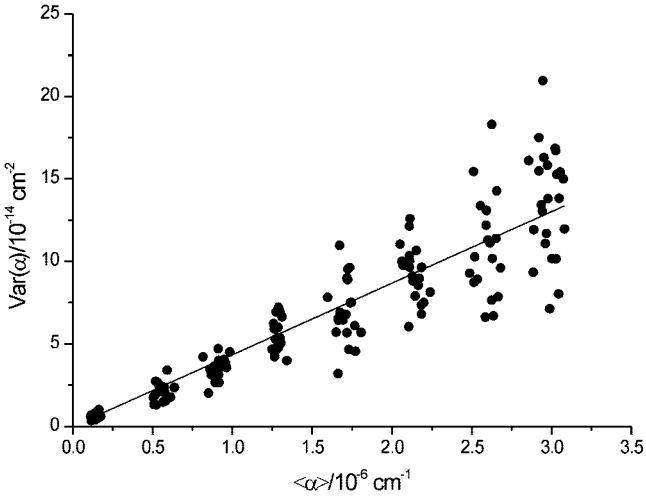

Figure 2. Simulated plot of $Var(\alpha)$ against $\langle\alpha\rangle$ for 1 μm diameter PSS particles. The equation of the fitted line is $Var(\alpha) = 4.38 \times 10^{-8} \langle\alpha\rangle$.

components. The direction of Brownian motion is randomly sampled at each time step (δt), and the particles move a distance determined by the mean-squared value

$$\langle(\delta r)^2\rangle = 2D\delta t \tag{14}$$

where D is a diffusion coefficient

$$D = \frac{kTC_c}{3\pi\eta d} \tag{15}$$

Here, η is the viscosity of the surrounding air, k is the Boltzmann constant, and C_c is a slip correction factor that depends on particle diameter and accounts for a drag force on the particle that is smaller than predicted by Stokes' Law. Values of the slip correction factor for different particle diameters are tabulated by Seinfeld and Pandis.[40]

The drift velocity under gravity and in the presence of friction, which is described by a coefficient f, is

$$v_{\text{grav}} = \frac{m_p g}{f} = \frac{m_p g C_c}{3\pi\eta d} \tag{16}$$

Figure 2 shows the results of a simulation for 1 μm diameter particles with a mean Brownian motion speed (per step) of 7.36×10^{-4} cm s^{-1} and a downward velocity under gravity of 3.64×10^{-3} cm s^{-1}. The simulation is carried out for an intracavity laser beam that mimics our experimental conditions (with beam radius $w = 0.45$ mm). We note that, with particles undergoing only Brownian motion and gravitational settling, average transit times through the beam are on the order of 25 s. The data in the figure are plotted as calculated $Var(\alpha)$ against $\langle\alpha\rangle$ to imitate the experimental data but employed a time-step interval of 2 s, together with analysis of 300 separate distributions to obtain each $Var(\alpha)$ and $\langle\alpha\rangle$ value. The increasing scatter in $Var(\alpha)$ values with $\langle\alpha\rangle$ that is observed is a consequence of the Poisson statistical nature of the system. Under the above conditions, the fitted gradient ($4.34 \pm 0.08 \times 10^{-8}$ cm^{-1}) agrees well with the expected value of $\sigma/V = 4.41 \times 10^{-8}$ cm^{-1}. If the time-step value is reduced but the same number of events are analyzed to obtain a variance, however, the gradient of the plot is also reduced because the determined variances are smaller. This result indicates a degree of correlation between the sampled distributions if the time interval is not sufficiently large. We will return to this point in the discussion of experimental results.

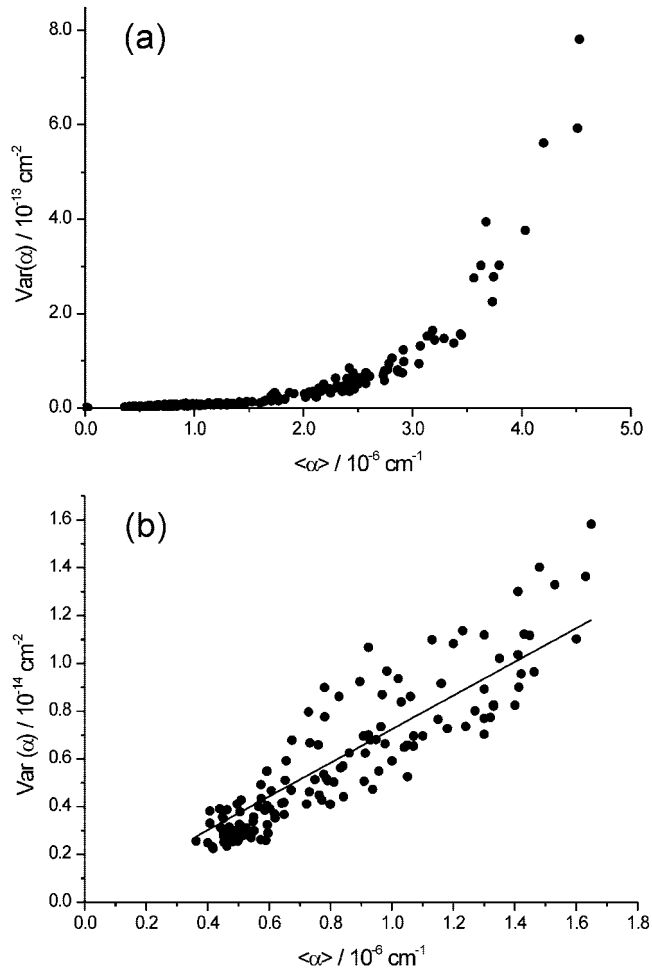

Figure 3. (a) Plot of $Var(\alpha)$ against $\langle\alpha\rangle$ for 700 nm PSS particles. (b) Expanded plot of the data for mean extinctions in the range up to $\langle\alpha\rangle = 1.8 \times 10^{-6}$ cm^{-1}. The analysis of the fitted straight line is discussed in the text.

4. Results and Discussion

4.A. Analysis of Extinction Data for Polystyrene Spheres. Four samples of polystyrene spheres were separately subjected to analysis to determine extinction cross sections using the method outlined in the preceding section, and the results are compared to expectations from Mie scattering theory. The samples used will be referred to as 700, 600, 500, and 400 nm beads; more precisely, the mean diameters and standard deviations (expressed as an uncertainty), as specified by the manufacturer, were 707 ± 8.5, 596 ± 7.7, 499 ± 6.5, and 404 ± 5.9 nm. Aqueous solutions of each PSS sample were nebulized, dried, and passed into the ring-down cavity chamber, and the extinction was measured while the number density varied over time. Values of $\langle\alpha\rangle$ and $Var(\alpha)$ were obtained from the rapid measurement of 500 ring-down events at each number density, and examples of the resultant data are plotted in Figure 3 for the 700 nm beads. An extinction coefficient $\alpha = 1.0 \times 10^{-6}$ cm^{-1} corresponds to ~125 of the 700 nm PSSs in the intracavity laser volume; the equivalent numbers for 600, 500, and 400 nm diameter beads required to produce this extinction coefficient are, respectively, 290, 770, and 2600 particles.

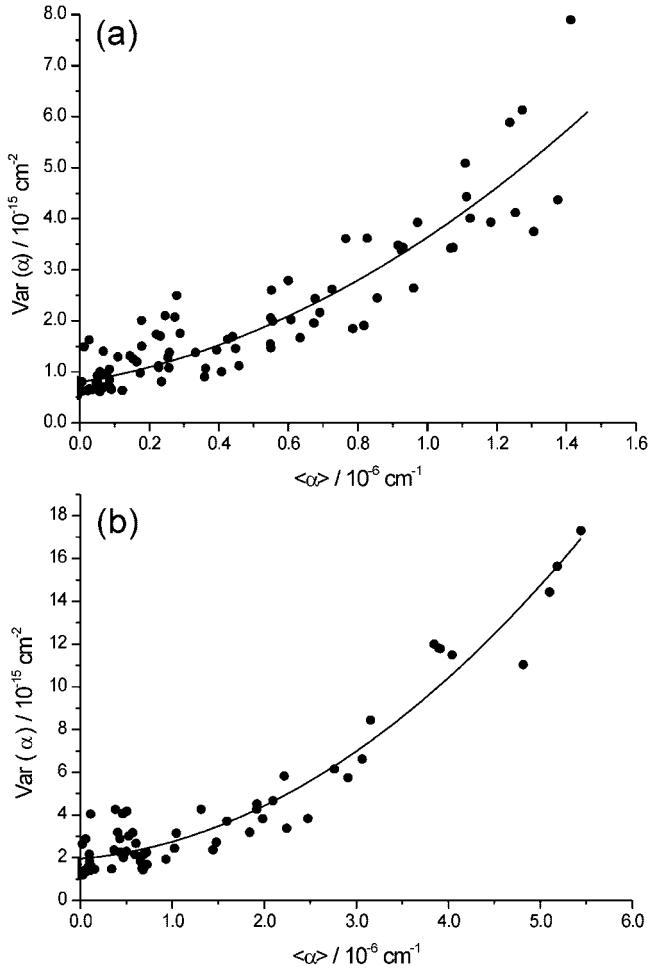

Figure 4. Plots of $Var(\alpha)$ against $\langle\alpha\rangle$ for (a) 500 nm PSS particles (the equation of the fitted line is $Var(\alpha) = 0.0016\langle\alpha\rangle^2 + 1.2 \times 10^{-9}\langle\alpha\rangle + 7.7 \times 10^{-16}$) and (b) 400 nm PSS particles (the fitted line gives $Var(\alpha) = 0.0043\langle\alpha\rangle^2 + 4.1 \times 10^{-10}\langle\alpha\rangle + 1.9 \times 10^{-15}$).

The experimental results show a relationship between $Var(\alpha)$ and $\langle\alpha\rangle$ that deviates from linearity for extinction coefficients greater than $\sim 2 \times 10^{-6}$ cm^{-1}. This nonlinearity is a consequence of aspects of the experimental method such as the uncertainty arising from fits to experimental ring-down decays (particularly for small values of the ring-down time) and is discussed in detail later. Figure 3 also demonstrates that for small values of the extinction coefficient ($\langle\alpha\rangle < 1.8 \times 10^{-6}$ cm^{-1}) the relationship between $Var(\alpha)$ and $\langle\alpha\rangle$ appears linear, and the extinction cross-section per particle can be deduced. A linear fit to the data, in which the intercept was constrained to the background noise level and the gradient was floated, gives $Var(\alpha) = 7.04 \times 10^{-9}\langle\alpha\rangle + 2.00 \times 10^{-16}$ with an uncertainty in the gradient of 1.3×10^{-10} cm^{-1}. Analysis of the gradient gives an extinction cross-section value of $\sigma_{exp} = (2.63 \pm 0.05) \times 10^{-9}$ cm^2. The calculation of this value employed an intracavity volume for the laser beam of $V = 0.374$ cm^3 (see section 3.A.3), which takes into account the partial focusing of the beam (eq 12). As noted earlier, in using this value of V in the analysis, we assume that the folded cavity used in the experiments behaves like a pair of linear cavities, with negligible overlap volume, and that the statistical formulation of eq 7 can be applied to a cavity mode that is not fully cylindrical with uniform radius.

Figure 4 shows equivalent plots of $Var(\alpha)$ against $\langle\alpha\rangle$ for the 500 and 400 nm diameter PSSs. Again, deviations from linearity are observed at higher extinction coefficient values and will be discussed later, but fits to the regions corresponding to low cavity losses were used to derive extinction cross-section values. Quadratic functions were employed to describe the data sets, with the intercept, linear, and quadratic fit parameters floated. Table 1 summarizes the experimental extinction cross-sections obtained for the these and the 700 nm sets of particles at a wavelength of 1650 nm, together with the uncertainties derived from the fits, and compares the experimental results with values obtained from Mie scattering calculations (σ_{calc}) using MiePlot v3.4.16 software.[41]

TABLE 1: Comparison of Experimentally Determined and Calculated Extinction Cross-sections for the Samples of 400−700 nm Diameter Polystyrene Spheres

particle diameter/nm	size parameter	$\sigma_{exp}/10^{-9}$ cm^{2a}	$\sigma_{calc}/10^{-9}$ cm^2	fractional difference
707 ± 8.5	1.35 ± 0.01	2.63 ± 0.05	2.97 ± 0.18	14%
596 ± 7.7	1.13 ± 0.01	0.71 ± 0.05	1.27 ± 0.09	79%[b]
499 ± 6.5	0.95 ± 0.01	0.45 ± 0.12	0.485 ± 0.036	8%
404 ± 5.9	0.77 ± 0.01	0.15 ± 0.07	0.146 ± 0.013	3%

[a] Uncertainties are those derived from the linear terms in the fits. Results for 404 and 499 nm diameter beads were derived from the linear coefficients in the quadratic fits to the data shown in Figure 4 and thus have larger fractional uncertainties. [b] Reasons for the large discrepancy with this data set are discussed in the main text.

The data shown in Figure 5 were obtained for 600 nm particles and illustrate a potential pitfall of the method for determination of extinction cross-sections from $Var(\alpha)$ data. The equation of the best fit line to the data is $Var(\alpha) = 1.89 \times 10^{-9}\langle\alpha\rangle + 6.80 \times 10^{-16}$, giving an intercept that is consistent with expectations for α_{min} for our apparatus but a gradient that is a factor of $\sim$2 smaller than the expected value of $\sigma/V = 3.3 \times 10^{-9}$ cm^{-1}. Monte-Carlo simulations of the type described in section 3.A.5 were carried out for this size of particle using an acquisition rate of 1 kHz but with particle speeds set to be 500 times faster than their calculated values based on Brownian motion and gravitational settling. Analysis of the simulated data in the form of a plot of $Var(\alpha)$ against $\langle\alpha\rangle$ gave a gradient of 1.8×10^{-9} cm^{-1}, which is in good agreement with the experimentally determined value. Increasing the particle speeds by a further factor of 4 in the simulations further increased the computed variances and gave a gradient in quantitative agreement with the expected value of σ/V (both are 3.3×10^{-9} cm^{-1}). We thus deduce that under our experimental conditions, the particles are moving much more quickly than predicted solely on the basis of Brownian motion and gravitational settling. These greater speeds are a necessary component of the experiments to ensure that sequential measurements of the optical extinction are not correlated (i.e., the distribution of particles must be completely refreshed between each measurement by motion into and out of the TEM_{00} mode volume). It appears that the data obtained for the 400, 500, and 700 nm diameter particles were close to this condition of uncorrelated measurements but that the 600 nm PSS data (taken at a time interval of several weeks after the other data sets) had some residual correlation between measurements, resulting in systematically low $Var(\alpha)$ data. The cause of faster motions of the particles than calculated by Brownian motion and gravitational settling might be residual motion of air in the chamber caused by introduction of the aerosol samples or convection currents. An adaptation to the experiment to incorporate fluorescence imaging of the motions of single particles is planned to explore this issue further.

4.B. Additional Sources of Variance in the Experimental Data. The data plotted in Figures 3 and 4 exhibit the expected linear relationship between $Var(\alpha)$ and $\langle\alpha\rangle$ for low values of $\langle\alpha\rangle$, but one or more additional sources of variance become

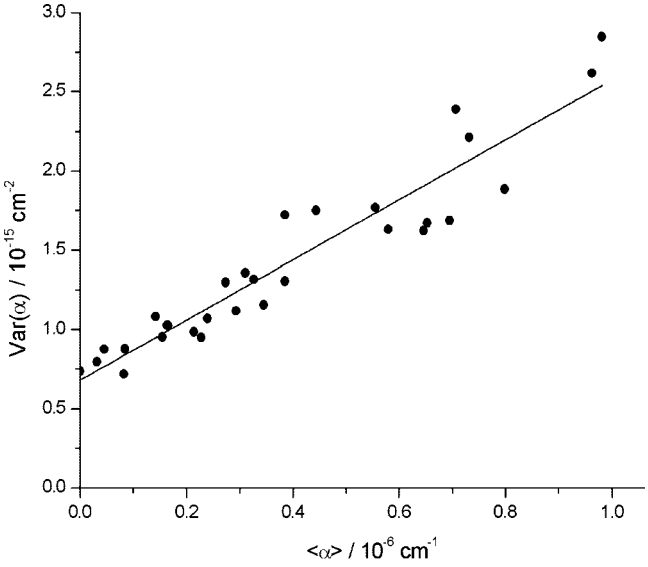

Figure 5. Plot of $Var(\alpha)$ against $\langle\alpha\rangle$ for 600 nm diameter PSS particles. The equation of the fitted line is $Var(\alpha) = 1.89 \times 10^{-9}\langle\alpha\rangle + 6.80 \times 10^{-16}$.

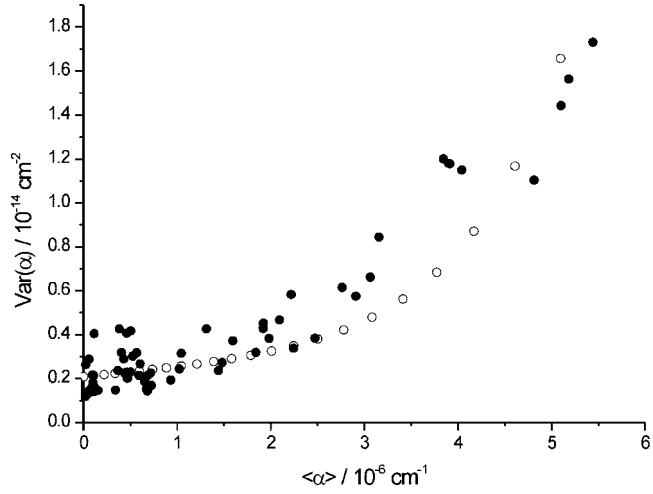

Figure 6. Comparison of the experimental data (●) for 400 nm PSS particles (from Figure 4b) with simulated data (○) obtained by combining contributions to $Var(\alpha)$ from the statistical fluctuations in particle numbers (in accord with eq 7), extinction-dependent reduction in cavity finesse (eq 18), and fitting of ring-down decays with an initial signal-to-noise ratio of 600 (eq 17), modified by the effect of neglecting the first 8 μs of the exponential decay.

pronounced at higher extinctions (corresponding to higher number densities of particles in the ring-down cavity). We first consider the additional variance that is introduced from the analysis of experimental ring-down decays. The data analysis program used a fast Fourier transform (FFT) fitting method[37] to derive ring-down rate coefficients (k); this method was chosen because it is sufficiently fast to cope with the high repetition rates of the experiment. Huang and Lehmann[42] showed that the variance in the extinction coefficient resulting from the FFT fitting method is

$$Var_{\mathrm{FFT}}(\alpha) = \frac{\Delta t^2(k^2 + \omega^2)^3 N_{\mathrm{p}}}{2\omega^2 c^2}\left(\frac{\sigma_A}{A}\right)^2 \qquad (17)$$

where Δt is the time interval between points in the exponential decay (determined by the digitization rate of the data acquisition equipment), N_{p} is the number of points analyzed in the decay, $\omega = 2\pi/N_{\mathrm{p}}\Delta t$ is the frequency component of the discrete Fourier transform used to extract a ring-down rate constant, c is the speed of light, A is the amplitude of the decay trace, and σ_A is the noise level on the exponential decay. This amplitude noise is mostly introduced from the detector and signal processing electronics. Typical values of the various parameters of eq 17 for our experimental conditions are $\Delta t = 4.0 \times 10^{-8}$ s, $N_{\mathrm{p}} = 1000$, $k = 1.25 \times 10^5$ s^{-1}, $\omega = 1.57 \times 10^5$ s^{-1}, and $A/\sigma_A \approx 1200$ (for the amplitude at the start of the ring-down decay).

The variance resulting from the ring-down decay fits can be calculated straightforwardly as a function of α if we assume that the noise level remains constant (i.e., a detector-noise-limited rather than a shot-noise-limited regime). There are two experimental reasons why the signal-to-noise ratio (SNR) varies with $\langle\alpha\rangle$, however, that are specific to the way our OF-CRDS experiments are conducted and require further consideration to account for greater contribution to $Var(\alpha)$ from the fitting method at high values of $\langle\alpha\rangle$. First, as α increases, the maximum build-up of light in the cavity (and thus the transmission intensity, which determines the value of A) decreases as a result of the greater cavity losses and associated reduction in the cavity finesse. This general effect has been quantified by Morville et al.[34] Second, the fits to individual ring-down decays exclude the first 8 μs because this early region does not fit well to a single-exponential function: the slow response of the diode laser current controller contributes a non-negligible delay to the switch-off of the light from the laser at the end of each voltage pulse. The amplitude of the decay in the region that is fitted is thus a factor of ~2 lower than the maximum amplitude of the decay trace, serving to decrease the overall A/σ_A ratio.

The various contributions to $Var(\alpha)$ arising from the CRD fitting procedure can be numerically simulated. Morville et al.[34] demonstrated that the intensity transmission function for a symmetric V-shaped optical cavity tuned into resonance with the incident laser beam and containing a sample that causes extinction is

$$I(\alpha) = I(\alpha = 0)\left(\frac{2(1 - R)\exp[-\alpha L/2]}{1 - R^2\exp[-2\alpha L]}\right)^2 \qquad (18)$$

Here we assumed negligible losses of light within the cavity mirrors and in coupling of the injected light to the TEM_{00} mode, so that $R = 1 - T$, where T is the mirror transmission. The effect of starting the fit at a given time delay after initiation of a ring-down event can be accounted for by scaling the amplitude by a factor deduced from an exponential decay with time constant $k = 1/\tau$. These corrections were incorporated into eq 17 and the values of $Var_{\mathrm{FFT}}(\alpha)$ evaluated for various $\langle\alpha\rangle$ values representative of our experiments. The results of these simulations are shown in Figure 6 for 400 nm PSSs and account satisfactorily for the curvature of the data sets plotted in Figures 4 and 6.

Introduction of variance from the analysis of the ring-down decays at high extinctions is not simply a consequence of our choice of the FFT fitting method. Weighted least-squares fitting is also commonly used in analysis of CRD events to obtain ring-down rate coefficients and times. Lehmann and Huang[42] showed that, when working in the detector-noise limit, the weighted least-squares fitting method introduces a variance

$$Var_{\mathrm{WLS}}(\alpha) = \left(\frac{\xi P_N}{A}\right)^2 \frac{(1 - e^{-k\Delta t})^3}{c^2 \Delta t^3 e^{-2k\Delta t}} \left[\frac{N_p(1 - e^{-k\Delta t}) - (1 + e^{-k\Delta t})}{N_p(1 - e^{-k\Delta t}) - 2(1 + e^{-k\Delta t})}\right] \quad (19)$$

where ξ is the excess noise over the ideal limit and P_N is the intrinsic detector noise. The excess noise is related to the response time of the detector and the time interval between points; a representative value for our experimental conditions is $\xi \approx 1.6$. Our simulations demonstrate that the additional variances introduced by the FFT and weighted least-squares fitting methods are comparable. The Levenberg−Marquardt method of fitting ring-down decays might reduce the variance from the fits but is not practical for our experiments because of its much slower computational speed.

The data shown in Figure 3a for 700 nm PSS particles exhibit $Var(\alpha)$ values that are much higher than can be explained in terms of the fluctuations in particle numbers and the fitting procedures for the ring-down decays. We speculate that the additional variance is caused by adhesion of particles to form dimers and perhaps also larger aggregates. To test this hypothesis, we carried out simulations of the experimental data in which we included 0−10% of spherical particles of diameter 1.4 μm. The simulations account successfully for the observed behavior if we allow the fraction of larger particles to increase as the total number of particles increases (i.e., as $\langle\alpha\rangle$ becomes larger); the values used for the simulated data in Figure 7 are summarized in the figure caption.

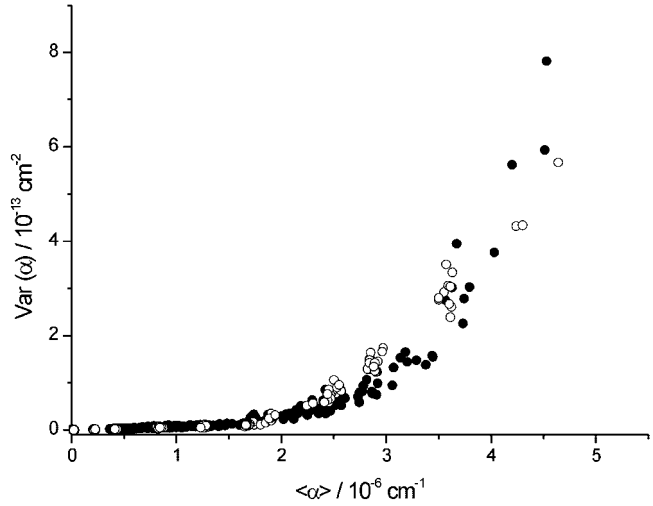

Figure 7. Comparison of the experimental data (●) for 700 nm PSS particles (from Figure 3a) with simulated results (○) that take into account the possible adhesion of particles to form dimers. In the simulations, the dimers were treated as spherical particles of diameter 1.4 μm, and the fractional abundance increased with total particle number density (and thus $\langle\alpha\rangle$) from 0% for $\langle\alpha\rangle < 1.8 \times 10^{-6}$ cm^{-1} to 1% for $\langle\alpha\rangle = 1.8 \times 10^{-6}$ to 3.0×10^{-6} cm^{-1}, 5% for $\langle\alpha\rangle = 3.0 \times 10^{-6}$ to 4.0×10^{-6} cm^{-1}, 6.8% for $\langle\alpha\rangle = 4.0 \times 10^{-6}$ to 4.5×10^{-6} cm^{-1}, and 10% for $\langle\alpha\rangle > 4.5 \times 10^{-6}$ cm^{-1}.

5. Conclusions

OF-CRDS has been used to measure the extinction caused by multiple, nearly monodisperse aerosol particles, and a statistical model has been developed to determine the extinction cross-section per particle without requirement of knowledge of the number density of particles in the sample.

The extinction cross-section per particle is determined by plotting the variances of the extinction coefficient against the mean values from experimental determinations and requires knowledge of the volume of the mode of the high-finesse optical cavity. For a TEM_{00} mode, this volume can be calculated straightforwardly. The relationship between $Var(\alpha)$ and $\langle\alpha\rangle$ deviates from linearity for extinction coefficients greater than $\sim 1 \times 10^{-6}$ cm^{-1} for our experimental conditions because of additional variance introduced by the fitting of exponential ring-down decays to extract ring-down rate coefficients. For smaller values of the extinction coefficient, the variance is dominated by fluctuations in the number of particles within the intracavity mode beam volume, and analysis using Poisson statistics enables determination of extinction cross-section values that agree well with the results of Mie theory calculations. The measurements must, however, be of uncorrelated distributions of the particles within the cavity or the values for $Var(\alpha)$, and thus, the extinction cross-sections are significantly underestimated. If Brownian motion and gravitational settling of the particles determine their speeds, the measurements must be made at low (<1 Hz) repetition rates to ensure the correct statistical behavior. Air currents in the sample resulting from convection or enforced air flow serve to refresh the distributions more rapidly and enable data accumulation rates at ~1 kHz frequencies.

Developments of the experimental method are underway that aim to improve the precision and accuracy of the σ_{exp} values and which are guided by computer simulations. The experimental results suggest that the method can be used to measure optical properties of aerosol samples of unknown composition, as long as a narrow range of sizes of particles is first selected, for example, using a differential mobility analyzer. Scanning the output sizes using the DMA should then provide extinction efficiencies as a function of particle diameters, which in turn provide information on the real and imaginary components of the refractive indices and the compositions of the particles. The analysis is, so far, restricted to spherical particles; whether quantitative information can be extracted from nonspherical particles remains to be established.

Acknowledgment. The authors are grateful to the EPSRC (grant EP/E018297), NERC (DIAC grant NER/S/R/2004/13085), and AWE for financial support. We thank Dr. J. L. Miller for important contributions to the early stages of this project and Dr. J. P. Reid, Dr. S. Rudić and R.E.H. Miles (University of Bristol) for helpful discussions. We are grateful to Prof. K. K. Lehmann (University of Virginia) for valuable discussions and correspondence concerning uncertainties in fitting ring-down decays. J.L. thanks the Natural Sciences and Engineering Research Council of Canada (NSERC) for funding for her visit to Bristol.

References and Notes

(1) Forster, P.; Ramaswamy, V.; Artaxo, P.; Berntsen, T.; Betts, R.; Fahey, D. W.; Haywood, J.; Lean, J.; Lowe, D. C.; Myhre, G.; Nganga, J.; Prinn, R.; Raga, G.; Schulz, M.; Van Dorland, R. Changes in Atmospheric Constituents and in Radiative Forcing. In *Climate Change 2007: The Physical Science Basis. Contribution of Working Group I to the Fourth Assessment Report of the Intergovernmental Panel on Climate Change*; Solomon, S., Qin, D., Manning, M., Chen, Z., Marquis, M., Averyt, K. B., Tignor, M., Miller, H. L., Eds.; Cambridge University Press: Cambridge, U.K. and New York, 2007.

(2) O'Keefe, A.; Deacon, D. A. G. *Rev. Sci. Instrumen.* **1988**, *59*, 2544.

(3) Busch, K. W.; Busch, M. A. *Cavity-ringdown spectroscopy: an ultratrace-absorption measurement technique*; American Chemical Society: Washington, DC, 1999.

(4) Wheeler, M. D.; Newman, S. M.; Orr-Ewing, A. J.; Ashfold, M. N. R. *J. Chem. Soc., Faraday Trans.* **1998**, *94*, 337.

(5) Mazurenka, M.; Orr-Ewing, A. J.; Peverall, R.; Ritchie, G. A. D. *Annu. Rep. Prog. Chem., Sect. C: Phys. Chem.* **2005**, *101*, 100.
(6) Scherer, J. J.; Paul, J. B.; O'Keefe, A.; Saykally, R. J. *Chem. Rev.* **1997**, *97*, 25.
(7) Zalicki, P.; Zare, R. N. *J. Chem. Phys.* **1995**, *102*, 2708.
(8) Brown, S. S. *Chem. Rev.* **2003**, *103*, 5219.
(9) Berden, G.; Peeters, R.; Meijer, G. *Int. Rev. Phys. Chem.* **2000**, *19*, 565.
(10) Atkinson, D. B. *Analyst* **2003**, *128*, 117.
(11) Sappey, A. D.; Hill, E. S.; Settersten, T.; Linne, M. A. *Opt. Lett.* **1998**, *23*, 954.
(12) Smith, J. D.; Atkinson, D. B. *Analyst* **2001**, *126*, 1216.
(13) Thompson, J. E.; Smith, B. W.; Winefordner, J. D. *Anal. Chem.* **2002**, *74*, 1962.
(14) Bulatov, V.; Fisher, M.; Schechter, I. *Anal. Chim. Acta* **2002**, *466*, 1.
(15) Strawa, A. W.; Castaneda, R.; Owano, T.; Baer, D. S.; Paldus, B. A. *J. Atmos. Oceanic Tech.* **2003**, *20*, 454.
(16) Pettersson, A.; Lovejoy, E. R.; Brock, C. A.; Brown, S. S.; Ravishankara, A. R. *J. Aerosol Sci.* **2004**, *35*, 995.
(17) Moosmuller, H.; Varma, R.; Arnott, W. P. *Aerosol Sci. Technol.* **2005**, *39*, 30.
(18) Strawa, A. W.; Elleman, R.; Hallar, A. G.; Covert, D.; Ricci, K.; Provencal, R.; Owano, T. W.; Jonsson, H. H.; Schmid, B.; Luu, A. P.; Bokarius, K.; Andrews, E. *J. Geophys. Res.-Atmos.* **2006**, 111.
(19) Baynard, T.; Lovejoy, E. R.; Pettersson, A.; Brown, S. S.; Lack, D.; Osthoff, H.; Massoli, P.; Ciciora, S.; Dube, W. P.; Ravishankara, A. R. *Aerosol Sci. Technol.* **2007**, *41*, 447.
(20) Thompson, J. E.; Nasajpour, H. D.; Smith, B. W.; Winefordner, J. D. *Aerosol Sci. Technol.* **2003**, *37*, 221.
(21) Vander Wal, R. L.; Ticich, T. M. *Appl. Opt.* **1999**, *38*, 1444.
(22) Thompson, J. E.; Barta, N.; Policarpio, D.; DuVall, R. *Opt. Express* **2008**, *16*, 2191.
(23) Rudić, S.; Miles, R. E. H.; Orr-Ewing, A. J.; Reid, J. P. *Appl. Opt.* **2007**, *46*, 6142.
(24) Bulatov, V.; Chen, Y. H.; Khalmanov, A.; Schechter, I. *Anal. Bioanal. Chem.* **2006**, *384*, 155.
(25) Spindler, C.; Riziq, A. A.; Rudich, Y. *Aerosol Sci. Technol.* **2007**, *41*, 1011.
(26) Butler, T. J. A.; Miller, J. L.; Orr-Ewing, A. J. *J. Chem. Phys.* **2007**, *126*, 174302.
(27) Miller, J. L.; Orr-Ewing, A. J. *J. Chem. Phys.* **2007**, *126*, 174303.
(28) Riziq, A. A.; Erlick, C.; Dinar, E.; Rudich, Y. *Atmos. Chem. Phys.* **2007**, *7*, 1523.
(29) Riziq, A. A.; Trainic, M.; Erlick, C.; Segre, E.; Rudich, Y. *Atmos. Chem. Phys.* **2008**, *8*, 1823.
(30) Dinar, E.; Riziq, A. A.; Spindler, C.; Erlick, C.; Kiss, G.; Rudich, Y. *Faraday Discuss.* **2008**, *137*, 279.
(31) Larsen, M. L. *J. Aerosol Sci.* **2007**, *38*, 807.
(32) Romanini, D.; Kachanov, A. A.; Sadeghi, N.; Stoeckel, F. *Chem. Phys. Lett.* **1997**, *264*, 316.
(33) Morville, J.; Romanini, D.; Kachanov, A. A.; Chenevier, M. *Appl. Phys. B: Lasers Opt.* **2004**, *78*, 465.
(34) Morville, J.; Kassi, S.; Chenevier, M.; Romanini, D. *Appl. Phys. B: Lasers Opt.* **2005**, *80*, 1027.
(35) Romanini, D.; Chenevier, M.; Kassi, S.; Schmidt, M.; Valant, C.; Ramonet, M.; Lopez, J.; Jost, H. J. *Appl. Phys. B: Lasers Opt.* **2006**, *83*, 659.
(36) Courtillot, I.; Morville, J.; Motto-Ros, V.; Romanini, D. *Appl. Phys. B: Lasers Opt.* **2006**, *85*, 407.
(37) Mazurenka, M.; Wada, R.; Shillings, A. J. L.; Butler, T. J. A.; Beames, J. M.; Orr-Ewing, A. J. *Appl. Phys. B: Lasers Opt.* **2005**, *81*, 135.
(38) Butler, T. J. A.; Mellon, D.; Orr-Ewing, A. J. *Faraday Discuss.* **2008**, *137*, 313.
(39) Siegman, A. E. *Lasers*; Oxford University Press: Oxford, 1986.
(40) Seinfeld, J. H.; Pandis, S. N. *Atmospheric chemistry and physics: from air pollution to climate change*, 2nd ed.; Wiley: Hoboken, NJ, 2006.
(41) Laven, P. MiePlot, v3.4.16 ed.; 2005.
(42) Lehmann, K. K.; Huang, H. Optimal Signal Processing in Cavity Ring-Down Spectroscopy. In *Frontiers of Molecular Spectroscopy*; Laane, J., Ed.; Elsevier: Amsterdam, 2008; Chapter 18.

JP810310B